Synthesis and Characterization of Xerogel Derived from Palm Kernel Shell Biochar and Comparison with Commercial Activated Carbon

Hadi Hamdi Mahdi[1], Ali Mohammed Saleh[1,2], Azil Bahari Alias[1*],
Ali H Jawad[3], Sami D. Salman[4], Deana Qarizada[1], Mostafa Mahmood Mostafa[5],
Noah Mohammed Saleh[2], Mahmod A. Abdulqader[1,6]

[1] School of Chemical Engineering, College of Engineering, University Technology MARA, Shah Alam, Selangor, 40450, Malaysia

[2] Renewable Energy Research Unit, Alhawija Institute, Northern Technical University, Iraq

[3] Faculty of Applied Sciences, University Technology MARA, 40450 Shah Alam, Selangor, Malaysia

[4] Department of Biochemical Engineering, Al-Khwarizmi College of Engineering, University of Baghdad, Iraq

[5] Directorate of Climate Change Ministry of Environment, Iraq

[6] Oil Products Distribution Company, Salahuldeen Branch, Tikrit, Ministry of Oil, Iraq

* Corresponding author's e-mail: azilbahari@uitm.edu.my

ABSTRACT

Biomass is an inexpensive adsorbent that has attracted considerable interest. The sol-gel process produced xerogel from palm kernel shell biochar (PKSB). This study aimed to synthesize and characterize palm kernel shell biochar xerogel (PKSBX) and compare it with commercial (AC). The synthesized xerogel, raw material, and AC were characterized using different characterization, including thermogravimetric analysis (TGA), X-ray diffraction (XRD), Fourier Transform Infrared Spectroscopy (FTIR), Brunauer-Emmett-Teller (BET), and Scanning Electron Microscopy (SEM). The FTIR spectrum analysis showed a wide range of bonds and confirmed the presence of C = C alkenes, amines N-H, and aromatic C-H functional groups. TGA analysis of samples was conducted at 10 °C/min. The thermal degradation of the sample undergoes several setups of loss mass. The degrades occurred between 50200 °C first setups, second between 200–700 °C, and third setups between 950–1000 °C. The surface morphological structure of each sample has been defined and compared using SEM data, which is further confirmed by XRD data. On the basis of on the characterization findings, it can be determined that the xerogel obtained from the synthesis process using PKSB as the raw material exhibits favorable characteristics for its potential usage as an adsorbent.

Keywords: xerogel, activated carbon, Palm Kernel shell biochar, sodium alginate.

INTRODUCTION

Recently, attention to climate change has been developed in the international community. It has encouraged the study of technologies aimed at reducing greenhouse gas emissions, including carbon dioxide CO_2, methane CH_4, nitrous oxide N_2O, and others, which contribute to global warming and climate change (Acevedo *et al.*, 2020). Paris agreement (PA) states that reducing global warming or the average global temperature to well below 2 °C and pursuing efforts to restrict it to 1.5 °C will control and avoid the dangers of climate change. CO_2 has been produced by rising energy demands from the industrial revolution until now, making it challenging to reduce the emissions of greenhouse gasses (GHG) (Sass and Wunderlich 2022). The world is facing global warming and climate change crises because of increasing GHG (mainly CO_2) atmospheric concentrations (Shen *et al.*, 2020). All facets of human activity

must include decarbonization in all sectors that produce CO_2 gas, from electricity generation to mobility, industry to the oil and gas sector, for the safety of the environment. CO_2 is generated by various anthropogenic activities, resulting in a concentration of up to 410 ppm in the atmosphere and the average global temperature increase to more than 1 °C (Yu *et al.*, 2012). According to the Intergovernmental Panel on Climate Change (IPCC), one of the most feasible options in the short term for reducing emissions of CO_2 is by adopting the political toward renewable energy and by implementing carbon capture storage (CCS) technologies. According to PA, The IPCC established an ambitious target of reducing carbon dioxide emissions by 50% by 2050 (Aresta and Dibenedetto 2010). There are various methods for CCS, including the absorption process by absorbents, Adsorption process by adsorbents (solid materials), cryogenics distillation, membrane technology, and cycles of carbonation-calcination (Zulkurnai *et al.*, 2017). Adsorption by solid material is preferable to other methods since it uses less energy and has lower production costs due to its higher selectivity (Zeng *et al.*, 2022). The most common adsorbents used in adsorption processes are porous solid material (activated carbon, zeolite, hydrogel, xerogel, and silica gel), which have been observed as one of the promising sorbents due to their stronger sorption capacity than the inorganic particle (Osagie *et al.*, 2021). Adsorbents must have favorable surface chemistry and a porous structure. Since CO_2 is an acidic gas, the surface of a solid carbonaceous material must be suitable to increase selectivity toward this gas (Lee and Park 2020). Over the last few decades, there has been significant development in new solid materials focusing on capturing harmful gases. Among these materials, porous solids in various forms have been recognized and widely implemented due to their large surface area and pore volume, allowing them to capture and store CO_2 molecules efficiently, such as activated carbon and xerogel.

Activated carbons are solid materials with a high porosity, making them extremely useful in carbon dioxide adsorption. This adaptability arises from their unique combination of textural qualities and surface chemistry. AC is widely recognized as a highly esteemed adsorbent in adsorption. It exhibits a remarkable surface area exceeding 1000 m²/g, mostly attributed to its extensive microporosity. The main advantages of AC as CO_2 adsorbents are their outstanding thermal conductivity, excellent thermal and chemical stability, and low precursor cost (Abd *et al.*, 2021). Likewise, biochar, is a solid material derived from the pyrolysis of biomass, it is a carbon material similar to an activated carbon which has a wide range of chemical compositions and surface properties depending on the production method, biomass type, activation conditions (Ahmad *et al.*, 2014). Biochar is successfully utilized to mitigate climate change, and remove various contaminants in aqueous solutions as an alternative adsorbent, including CO_2, excessive nutrients, and pharmaceuticals (Ahmad *et al.*, 2013a, b; Creamer *et al.*, 2014; Vithanage *et al.*, 2014). In comparison with an activated carbon, the manufacturing of biochar requires less energy and no pre- or post-activation processes, although it has a high adsorption ability and capacity (Sun *et al.*, 2014). Biochar is also a well-known means of carbon sequestration (Creamer *et al.*, 2014). Different biomass precursors were utilized for biochar preparation using various activating agents with different activation ratio and activation temperatures for CO_2 adsorption, illustrated in Table 1.

Nowadays, worldwide attention is attracted to producing porous materials (xerogel) via the sol-gel method and drying by oven. Xerogels are the new material from biomass waste that can replace AC. Xerogel is a unique material in terms of physical and chemical properties because it is hydrophilic. Xerogel is a type of biomaterial with a microporous structure, and low-density has various applications in industry. Xerogels are derived from gels by replacing the liquid phase, generally solvent crystals, with a gaseous phase while preserving the strength of the porous solid structure (Deana *et al.*, 2023). Xerogel-based palm kernel shell biochar is important, because it will develop into an efficient and affordable material used extensively worldwide as an absorbent. It effectively adsorbs engine oil, heavy metals from wastewater, and harmful gases (Imoisili *et al.*, 2020). The present study focused on synthesizing and characterizing a novel, cost-effective, and versatile xerogel derived from palm kernel shell biochar as an adsorbent capable of adsorbing CO_2 and comparison with commercial AC.

Table 1. Biochar produced from different biomass precursors for CO_2 adsorption

Biomass precursor	Activation agent	Activation ratio	Activation temp. (°C)	SBET (m^2/g)	Pore volume (cm^3/g)	References
Africa palm shells	KOH	3:1	600	1250	0.61	(Ello et al. 2013)
	H_3PO_4	NA	450	1942	0.42	(Vargas et al. 2011)
Almond shells	CO_2	-	750	822	0.37	(González García et al. 2013)
Coca shell	H_3PO_4	NA	450	1322	0.49	(Vargas et al. 2011)
Coconut shell	H_3PO_4	NA	650	1593	0.49	(Vargas et al. 2011)
Argon shell	KOH	NA	850	1880	0.87	(Boujibar et al. 2018)
Beer Waste	CO_2	-	800	622	0.317	(Hao et al. 2013)
	H_3PO_4	NA	600	1073	0.978	(Hao et al. 2013)
Camphor leaves	KOH	2:1	600	1146	0.546	(Xu et al. 2018)
Carrot peels	KOH	1:1	700	1379	0.58	(Serafin et al. 2017)
Coconut shell	KOH	1:1	650	1332	0.68	(Guo et al. 2016)
	H_3PO_4	1:1	650	1593	0.68	(Guo et al. 2016)
	KOH	1:1	650	1593	0.6	(Chen et al. 2016)
	KOH	1:1	650	1535	0.5649	(Yue et al. 2018)
	K_2CO_3	1:1	600	10822	0.39	(Yue et al. 2018)
Empty fruit brunch	KOH	5:1	800	2510	1.05	(Parshetti et al. 2015)
Lignin	KOH	NA	700	1647	0.69	(Han et al. 2019)
Fern leaves	KOH	1:1	700	1593	0.74	(Serafin et al. 2017)
	KOH	1:1	700	1593	0.74	(Serafin et al. 2017)
Garlic peel	KOH	2:1	600	967	0.51	(Huang et al. 2019)

MATERIALS AND METHODS

Materials

PKSB was used in this study as a raw material in the preparation of xerogel (PKSBX) and was sourced from Kuala Korai, Kelantan, 18000, Malaysia. Calcium carbonate ($CaCO_3$), sodium alginate, glucono-δ-lactone (GDL) were provided by the College of Engineering, School of Chemical Engineering. Distilled water was used to synthesize xerogel.

Methods

Preparation of palm kernel shell biochar

Palm kernel shell biochar (PKSB) was utilized as the raw material in the production of xerogel. PKSB was crushed using a mortar and pestle to produce particles ranging from 1 to 2 mm. Crushed PKSB weighing 2.88 g was used to create xerogel. The sol-gel method is used to prepare xerogel, and it consists of three primary steps: sol production, gelation and drying operations. In the first step, 4.13 g of sodium alginate was mixed with 500 mL of distilled water under the agitation of a magnetic stirrer until homogenized mixture was obtained. In the second step, the homogenized sodium alginate solution introduced 1.73 g of calcium carbonate and 2.88 g of PKSB. Subsequently, the gelation or polymerization process started by adding 4.58 g of GDL into the homogeneous solution. The hydrogel was synthesized and then transferred into a square mold, which was cooled at a temperature of 4 °C until the gelation process was completed. Finally, the hydrogel was extracted from the square mold and placed into an aluminum tray to prepare for drying. Then, the hydrogel sample will undergo the drying procedure (Lopes *et al.*, 2017). Figure 1 shows the main steps of xerogel preparation.

Xerogel drying method

The process of drying xerogel is facilitated through the utilization of oven drying. Oven drying is a solvent removal procedure that assists the transition of a hydrogel into a xerogel state. The hydrogel sample was subjected to a longer drying process at a low temperature in an oven. The oven-drying

Table 2. Biochar produced from different biomass precursors for CO_2 adsorption (continued)

Biomass precursor	Activation agent	Activation ratio	Activation Temp. (°C)	SBET (m²/g)	Pore volume (cm³/g)	References
Grass cuttings	CO_2	-	800	841	0.379	(Ahmad et al. 2014)
Hazelnut shell	KOH	1:1	550	1118	0.47	(Pang et al. 2020)
	KOH	1:1	650	1696	0.7	(Pang et al. 2020)
	KOH	1:1	660	1118	0.59	(Pang et al. 2020)
Horse manure	CO_2	-	800	749	0.816	(Ahmad et al. 2014)
Jujun grass	KOH	2:1	700	1512	0.74	(Coromina et al. 2016)
Olive mill waste	CO_2	-	850	1135	0.476	(González and Manyà 2020)
Olive mill waste	KOH	7:1	700	1036	0.449	(González and Manyà 2020)
Pine cone shell	KOH	2:1	650	3135	0.71	(Li et al. 2016)
	KOH	1:1	710	1041	0.53	(Deng et al. 2014)
Rice husk	KOH	1:1	700	1162	0.685	(Li et al. 2015)
Pomegranate peels	KOH	1:1	700	585	0.28	(Serafin et al. 2017)
Sargassum	KOH	1:1	700	291.8	0.24	(Ding & Liu 2020)
Sugarcane bagasse	KOH	2:1	600	1113	0.574	(Han et al. 2019)
Water caltrop shell	KOH	2:1	550	1275	0.55	(Zhao et al. 2021)
	KOH	2:1	550	1535	0.66	(Zhao et al. 2021)
	KOH	2:1	600	2194	1.01	(Zhao et al. 2021)
Water chestnut shell	KOH	0.9:1	550	1021	0.45	(Li et al. 2020)
	KOH	0.9:1	600	1296	0.66	(Li et al. 2020)
	KOH	0.9:1	6500	1517	1.08	(Li et al. 2020)
Pine cone shell	KOH	2:1	650	3135	0.71	(Li et al. 2016)
	KOH	1:1	710	1041	0.53	(Deng et al. 2014)
Rice husk	KOH	1:1	700	1162	0.685	(Li et al. 2015)
Pomegranate peels	KOH	1:1	700	585	0.28	(Serafin et al. 2017)
Sargassum	KOH	1:1	700	291.8	0.24	(Ding and Liu 2020)
Sugarcane bagasse	KOH	2:1	600	1113	0.574	(Han et al. 2019)
Water caltrop shell	KOH	2:1	550	1275	0.55	(Zhao et al. 2021)
	KOH	2:1	550	1535	0.66	(Zhao et al. 2021)
	KOH	2:1	600	2194	1.01	(Zhao et al. 2021)
Water chestnut shell	KOH	0.9:1	550	1021	0.45	(Li et al. 2020)
	KOH	0.9:1	600	1296	0.66	(Li et al. 2020)
	KOH	0.9:1	6500	1517	1.08	(Li et al. 2020)

procedure was conducted over three days at a temperature of 60 °C (Noraini *et al.*, 2022).

Characterizations procedure

Characterization was done to analyze the PKSB, the palm kernel shell biochar activated carbon (PKSBAC), and palm kernel shell biochar xerogel (PKSBX). Were via CHNS-O analysis, the samples were degassed for 1 hour at 90 °C and another 4 hours at 300 °C while circulated with N_2. At 77 K, isotherms for both N_2 adsorption and desorption were reached (Quan *et al.*, 2023). Brunauer-Emmett-Teller (BET) using an automatic surface analyzer device called the micromeritic 3 flex. The BET study used a sample weight ranging from 0.1g to 0.2 g, with a heat rate of 10 °C/min. The BET method utilizes a nitrogen (N_2) adsorption and desorption process at a 10 mL/min flow rate. This process is conducted at a temperature of 40 °C for 6 hours. Fourier Transform Infrared Spectroscopy (FTIR) It conforms
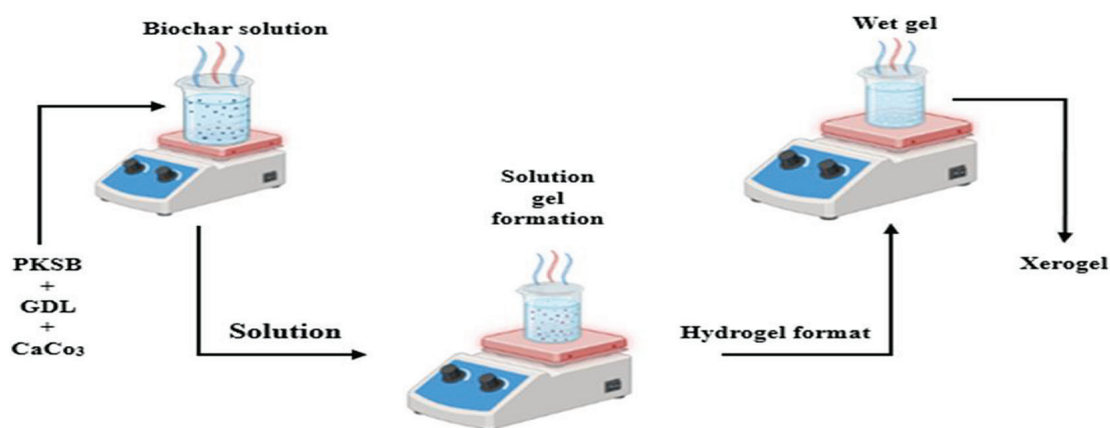
Figure 1. Main steps of xerogel preparation

with the standards specified in ASTM E1252-98. Consequently, FTIR was conducted using a Perkin Elmer Spectrum 2000 FTIR at 4000 to 600 cm^{-1} wavelength to examine the sample's structural composition change can scanning electron microscopy (SEM) images and X-ray diffraction. Thermogravimetric analysis (TGA) uses the ASTM standard method D5142-02a to investigate the stability of the material.

RESULTS AND DISCUSSION

Elemental analysis

The Perkin Elmer PE2400 Elemental Analyzer was utilized to conduct the comprehensive examination of nitrogen (N), hydrogen (H), carbon (C), sulfere (S) and oxegen (O). The textural qualities of the prepared samples were examined using the Micromeritics Tristar II 3020. The elemental analysis of PKSB, AC, and PKSBX, is described in Table 2. On the basis of the results, all samples have high carbon and oxygen content. AC has a higher carbon content than PKSB PKSBX, it depends on activation temperature. Increasing temperature activation increases carbon content due to the discharge of volatile matter. Xerogel is commonly produced by the sol-gel approach, in which a gel is formed from a precursor

solution and subsequently undergoes drying to eliminate the solvent. Throughout this process, it may be possible for chemical reactions to occur, which might cause the removal of functional groups containing carbon or organic constituents. Consequently, this results in a decrease in the overall carbon content shown in Table 3.

Brunauer-Emmett-Teller

BET method was used to characterize specific surface area (m^2/g), pore volume (m^3/g), and average pore size (nm) of the samples. The surface area was determined using the BET theory and equation, whereas the micropore volume was determined using the Dubinin-Radushkevich (DR) method (Al Malki *et al.*, 2023). The BET surface area, pore size, and pore volume of PKSB, PKSBX and AC are illustrated in Table 3. AC has a higher surface area 868 m^2/g, pore size 1.7532 nm, and pore volume 0.3805 m^3/g compared to PKSB 355.7066 m^2/g, pore size 2.0376 nm, pore volume 0.1820 cm^3/g and PKSBX 29.4535 m^2 surface area, pore size 4.6203 nm, and pore volume 0.0295 m^3/g. The xerogel properties decreased (Yasin *et al.*, 2021). The results indicated that the xerogel surface area, pore size, and pore volume decreased after the gelation process as shown in Table 4. All the pore size is blocked by gel. Furthermore, the

Table 3. Elemental analysis of PKSB, PKSBX, and PKSAC

Raw materials	C	H	N	S	O
PKSB	43.22	1.38	0.37	0.52	54.49
PKSBX	44.43	3.60	0.52	0.51	50.92
PKSAC	45.62	1.22	0.15	0.30	52.69

drying of the hydrogel may have induced shrinkage in the xerogel structure, resulting in a low surface area (Kumar and Jena 2016).

Fourier transform infrared spectroscopy

The chemical properties of PKSB, PKSBAC, and PKSBX were investigated using FTIR analysis to investigate their chemical characteristics and functional groups. Figure 2 illustrates the impact of PKSB, AC, and PKSBX on the surface functional groups investigated using FTIR analysis. The adsorption capacity of PKSB, AC, and PKSBX is determined by porosity and the chemical reactivity of surface functional groups. Various functional groups on the adsorbent surface contribute to carbon's preferential adsorption of different molecule species (Supian *et al.*, 2020). All wavelengths demonstrate a wide range in the 3378.73 cm^{-1} to 3474.20 cm^{-1} region, corresponding to N-H stretching and aliphatic primary amines (Kunusa *et al.*, 2021). Furthermore, the wave in the region of 2032.76 cm^{-1}- 2048.74 cm^{-1} is due to C-H bounding demonstrated aromatic compounds. The peak increase in PKSBX may be due to the chemicals during synthesis (Alias and Qarizada 2022). At

waves 1625.44 cm^{-1}, 1627.19 cm^{-1} and 1633.80 cm^{-1}, peaks in the wave spectrum of PKSB, PKSAC, and PKSBX corresponding to C = C show the alkene group (Maulina and Mentari 2019).

Scanning electron microscopy

Figure 3 shows the SEM images of (a) PKSB, (b) AC, and (c) PKSBX. PKSB samples are very fibrous and irregular, with limited structure. To ensure the accuracy test before the SEM imaging, a gold layer was used on all samples to remove residual ions. This device captures images by observing how fiber and samples tend to bond together using backscattered electron imaging (BSE). In addition, SEM analysis could identify the opened pores in a sample, whatever their size (Amosa 2015). The surface morphology of the sample exhibits a high level of magnification, indicating the presence of irregular stone formations. A crack structure like a bone skeleton and pores facilitating gas adsorption is also observed. The AC images show several small white particles, and the sample had a hollow shape; even though the number of pores produced was small because there were still many impurities, they closed the pores of the AC (Glaser *et al.*, 2021). The depolymerization and release of volatile chemicals from organic compounds during the carbonization process cause pore size and shape variations on the surface of AC ("Research article production and characterization of activated carbon from" 2018). The xerogel surface is more irregular and fibrous compared to PKSB. However, shrinkage is not unavoidable in xerogel at oven-drying temperatures. Therefore, less apparent

Table 4. BET analysis of PKSB, PKSAC and PKSBX

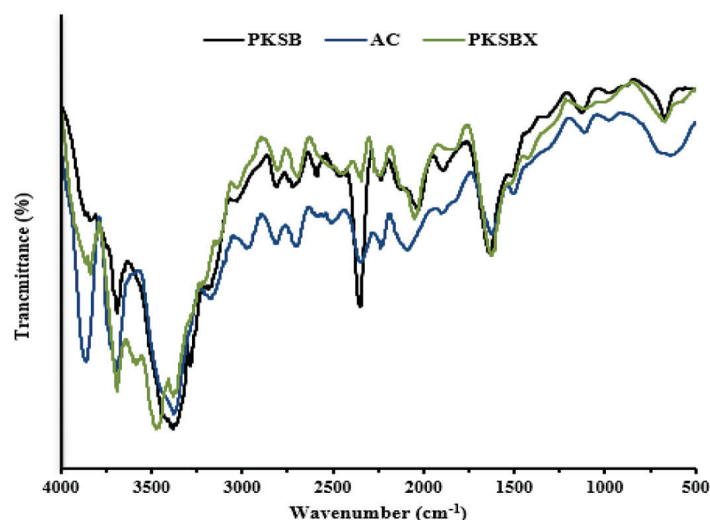| Properties	Surface area m²/g	Pore size nm	Pore volume cm³/g
PKSB	355.7066	2.0376	0.1820
PKSBX	29.4535	4.6203	0.0295
PKSAC	868	1.7532	0.3805

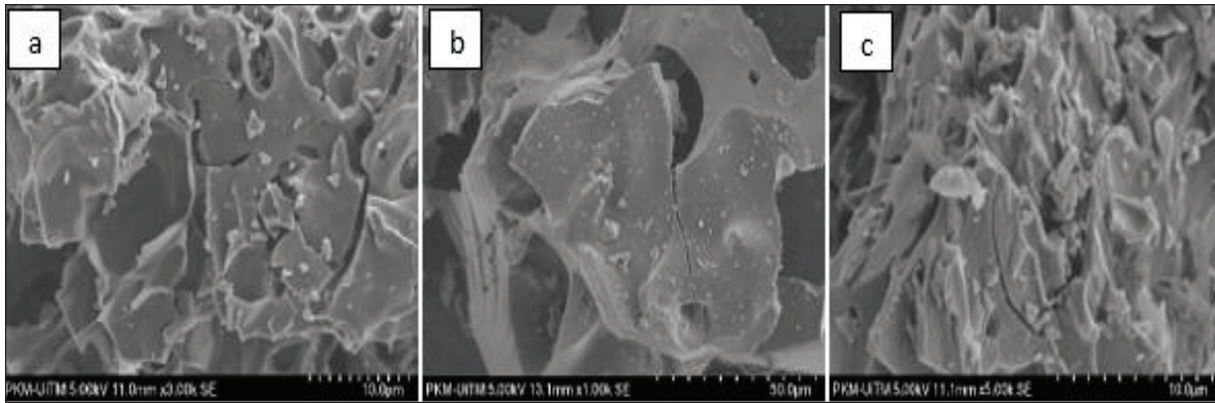**Figure 2.** FTIR analysis of PKSB, PKSAC, and PKSBX

Figure 3. SEM images of (a) PKSB, (b) PKSAC, and (c) PKSBX

pores were determined in xerogel. In addition, xerogel shows a highly complex network and rough surface (Wang *et al.*, 2016).

X-ray diffraction

X-ray diffraction (XRD) is a quick method of analysis used mostly for phase identification of crystalline materials and to confirm the presence of crystallinity in the investigated sample. The diffraction angle range of 2 Θ from 0° to 90° as a function of the intensity of the diffracted X-ray. Patterns are recorded at diffraction angles of 2Θ ranging from 5° to 60° at room temperature during the approximately 25 – minute analysis of the sample. The XRD analysis function measures the estimated PKSB, PKSBAC, and PKSBX analysis in a nitrogen atmosphere. The samples were analyzed at a starting temperature of 25 °C and

a final temperature of 600 °C, with a heating rate of 5 °C per minute, under nitrogen atmosphere. The gas flow was initiated at 25 ml/min (Segovia-sandoval *et al.*, 2019). Figure 4 demonstrates the XRD patterns of PKSB, PKSBX, and AC. Considering the peak intensities of the PKSB and AC samples, a small difference can be observed between 25 θ and 26 θ, whereas 100% of the intensities occur at 26θ. The diffraction pattern of PKSB AC, and PKSBX is classified as semi-crystalline diffraction or graphite material (Lee *et al.*, 2021). These findings demonstrate that most of the carbon consists of turbostratic structures. Furthermore, the pattern of carbons changes depending on the activation degree (Lee *et al.*, 2021). The XRD patterns of PKSBX provided a different perspective on the crystallinity of samples. This is due to the combination of chemicals used during the internal gelation process to produce PKSBX.
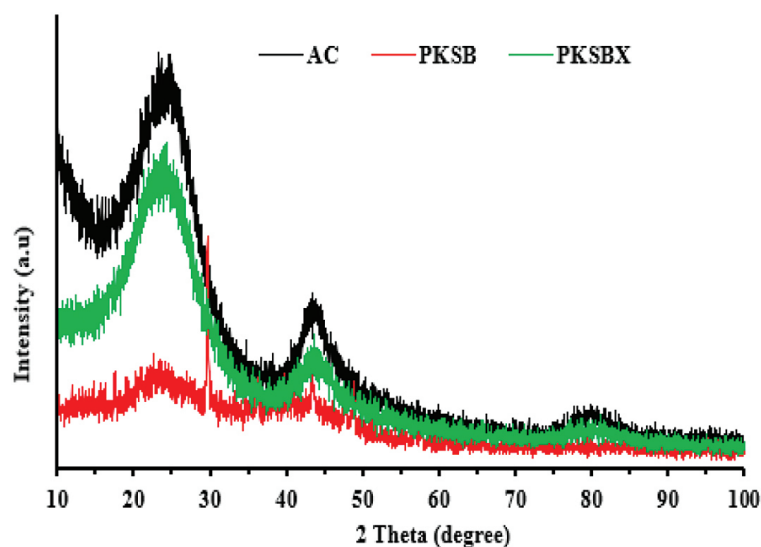

Figure 4. XRD patterns of PKSB, PKSBX, and PKSAC

The specific XRD patterns and interpretations depend on xerogel characteristics, composition, synthesis methodologies, and processing conditions. Xerogel are typically highly porous and amorphous in structure, but crystallinity may be observed depending on the synthesis conditions and processing techniques (Shah *et al.*, 2017).

Thermografmetric analysis

In order to determine the elemental composition of the materials, including moisture content, volatile matter content, and carbon content, the thermogravimetric method was employed utilizing the Mettler instrument. The TGA is a scientific instrument used for thermal analysis. The xerogel, activated carbon, and palm kernel shell (PKS) biochar samples underwent thermal treatment at a temperature of 950 °C, with a heating rate of 20 °C/min, in the presence of air inside a nitrogen environment. The gas flow rate was maintained at 100 ml/min. Subsequently, the provided sample environment is introduced into the surrounding air and subjected to a temperature elevation of 1200 °C [18]. TGA analysis of PKSB, PKSBX, and AC is illustrated in Figure 5. Up to 50 °C, the first stage mass loss PKSB 12.9% (1.2 mg) due to evaporation of water molecules. The second region response was the AC, losing 12.1% (1.1 mg). At the same time, the mass loss of PKSBX was 9.2% (0.9 mg). The main reason for this mass loss is the physical adsorption of water into the xerogel at the first stage of the TGA curve. Between 200 and 700 °C, mass loss is attributed to the release of volatile matter. The xerogel degrades, with 52.1% of the original mass (5.2 mg) lost in the second stage, followed by PKSB 16.2 % (1.6 mg) and AC 6.0% (0.6 mg). Significant mass loss in the xerogel sample is higher than that of PKSB and AC in step 2 due to the chemically bound water from the weight reduction due to chemically bonded water from the sol-gel
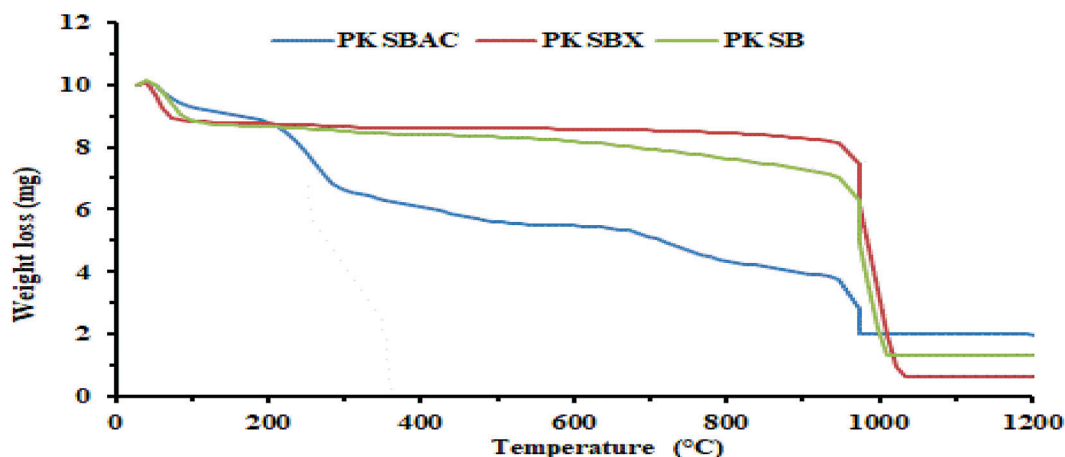

Figure 5. TGA analysis PKSB, PKSAC, and PKSBX

Table 5. Advantages and disadvantages of PKSBX compared to biochar

Advantages of PKSBX	Disadvantages of PKSBX
Xerogel-based PKS biochar typically exhibits superior porosity compared to conventional biochar. This increased porosity improves its adsorption capacity for various pollutants.	The production of xerogel-based biochar typically involves more complex and costly manufacturing processes compared to conventional biochar production methods. This higher cost may limit its widespread adoption, especially in large-scale applications.
The synthesis of xerogel-based biochar allows for the modification of its surface chemistry. This enables the customization of functional groups to enhance specific adsorption characteristics, providing better selectivity and efficiency in removing target pollutants.	The unique synthesis process of xerogel-based biochar may restrict its scalability for mass production. This limitation can present challenges when attempting to meet larger demand or when considering commercial viability.
Xerogel-based biochar production involves a controlled manufacturing process, resulting in consistent and reproducible material properties. This reliability in manufacturing ensures predictable adsorption performance and easier integration into industrial applications.	The manufacturing process of xerogel-based biochar may require the use of chemicals and energy-intensive procedures, potentially leading to higher carbon footprints compared to conventional biochar production. Ensuring proper waste disposal or recycling of chemicals used in the process is important to mitigate any negative environmental impacts.

manufacturing technique. The same result was reported by (Guzel and Deveci 2020). A notable mass loss of AC 74.9% (7.4 mg) is shown at 1050 °C after switching the atmosphere to oxidizing atmospheric air combustion. A mass loss of 56.5% (5.6 mg) is shown at temperatures between 950 and 1000 °C for PKSB, PKSBAC and a mass loss of PKSBX 17.9% (7.9 mg) at 950 °C, respectively. The last peak shows the thermal breakdown of carbon, while the remaining curve represents the amount of ash (Meri *et al.*, 2018). On the basis of the characterization of PKSB, PKSBX, and PKSAC, the advantages and disadvantages of the prepared PKSBX as compared to biochar produced from different biomass precursors are illustrated in Table 5.

CONCLUSIONS

The synthesis of xerogel via a sol-gel process as well as its characterization and comparison with commercialized PKSAC were investigated in this research. The xerogel was synthesized with 29.4535 m^2/g surface area, pore size 4.6203 nm, pore volume 0.0295 cm^3/g. The TGA analysis of xerogel illustrates that the volatile matter was reduced by 52.1% compared to PKSB by 16.2% and PKSAC 6% due to the chemically bound water from the weight reduction due to chemically bonded water from the sol-gel manufacturing technique. SEM images reveal that the xerogel exhibits a significantly complicated pore size, porous structure, and irregular surface. This can be attributed to its small pore size, which matches the characteristics of PKSB and AC. On the basis of FTIR analysis, functional groups N-H, C-H, and C=C were obtained in all three samples. XRD analysis confirmed that the produced xerogel is crystalline due to the chemicals, and PKSAC and PKSB showed semi-crystalline properties. Elemental analysis showed H content increased in xerogel compared to AC and biochar. On the basis of the results, the xerogel derived from PKSB can potentially adsorb toxic and CO_2 gases and have metals from wastewater and can be used as a cost-effective, environment-friendly adsorbent in industry. Xerogel and activated carbon are both versatile materials with different applications and properties. The selection between xerogel and activated carbon depends upon the specifications of the given application. In conclusion, xerogel is a suitable, cost-effective adsorbent for capturing CO_2.

REFERENCES

1. Acevedo S., Giraldo L. and Moreno-Piraján J. C. 2020. Adsorption of CO2 on activated carbons prepared by chemical activation with cupric nitrate, ACS omega, 5(18), 10423–10432.

2. Sass J. and Wunderlich R. 2022. Impact of Regulatory Requirements for Emission Trading Systems: An Analysis in a Stochastic Control Model.

3. Shen M., Huang W., Chen M., Song B., Zeng G., and Zhang Y. 2020. (Micro) plastic crisis: un-ignorable contribution to global greenhouse gas emissions and climate change, J. Clean. Prod., 254, 120138.

4. Yu C.-H., Huang C.-H. and Tan C.-S. 2012. A review of CO2 capture by absorption and adsorption, Aerosol Air Qual. Res., 12(5), 745–769.

5. Aresta M. and Dibenedetto A. 2010. Industrial utilization of carbon dioxide (CO2), in Developments and innovation in carbon dioxide (CO2) capture and storage technology, Elsevier, 377–410.

6. Zulkurnai N. Z., Ali U. F. M., Ibrahim N., and Manan N. S. A. 2017. Carbon dioxide (CO2) adsorption by activated carbon functionalized with deep eutectic solvent (DES), in IOP Conference Series: Materials Science and Engineering, IOP Publishing, 12001.

7. Zeng H., Qu X., Xu D. and Luo Y. 2022. Porous adsorption materials for carbon dioxide capture in industrial flue gas, Front. Chem., 10, 939701.

8. Osagie C., Othmani A., Ghosh S., Malloum A., Esfahani Z. K., and Ahmadi S. 2021. Dyes adsorption from aqueous media through the nanotechnology: A review, J. Mater. Res. Technol., 14, 2195–2218.

9. Lee J.-H. and Park S.-J. 2020. Recent advances in preparations and applications of carbon aerogels: A review, Carbon N. Y., 163, 1–18.

10. Abd A. A., Othman M. R., and Kim J. 2021. A review on application of activated carbons for carbon dioxide capture: present performance, preparation, and surface modification for further improvement, Environ. Sci. Pollut. Res., 28(32), 43329–43364.

11. Ahmad M., Lim J. E., Zhang M., Rajapaksha A. U. 2014. Biochar as a sorbent for contaminant management in soil and water: a review, Chemosphere, 99, 19–33.

12. Ahmad M., Al-Wabel M. I., Vithanage M., Rajapaksha A. U., Kim H. S., Lee S. S. and Ok. Y. S. 2013. Modeling adsorption kinetics of trichloroethylene onto biochars derived from soybean stover and peanut shell wastes, Environ. Sci. Pollut. Res., 20, 8364–8373.

13. Ahmad M., Lee S. S., Rajapaksha A. U., Vithanage M., Zhang, M. Cho J. S., Lee S.-E., Ok Y. S. 2013. Trichloroethylene adsorption by pine needle biochars produced at various pyrolysis temperatures, Bioresour. Technol., 143, 615–622.

14. Vithanage M., Rajapaksha A. U., Tang X.,

Thiele-Bruhn S., Kim K. H., Lee S.-E., Ok Y. S. 2014. Sorption and transport of sulfamethazine in agricultural soils amended with invasive-plant-derived biochar, J. Environ. Manage., 141, 95–103.

15. Creamer A. E., Gao B. and Zhang M. 2014. Carbon dioxide capture using biochar produced from sugarcane bagasse and hickory wood, Chem. Eng. J., 249, 174–179.

16. Sun Y., Bin Gao, Yao Y., Fang J. 2014. Effects of feedstock type, production method, and pyrolysis temperature on biochar and hydrochar properties, Chem. Eng. J., 240, 574–578.

17. Ello A. S., de Souza L. K. C., Trokourey A. and Jaroniec M. 2013. Development of microporous carbons for CO2 capture by KOH activation of African palm shells, J. CO2 Util., 2, 35–38.

18. Vargas D. P., Giraldo L., Silvestre-Albero J. and Moreno-Piraján J. C. 2011. CO2 adsorption on binderless activated carbon monoliths, Adsorption, 17, 497–504.

19. González García A. S., González Plaza M., Rubiera González F. and Pevida García C. 2013. Sustainable biomass-based carbon adsorbents for post-combustion CO2 capture,.

20. Boujibar O., Souikny A., Ghamouss F., Achak O., Dahbi M., and Chafik T. 2018. CO2 capture using N-containing nanoporous activated carbon obtained from argan fruit shells, J. Environ. Chem. Eng., 6(2), 1995–2002.

21. Hao W., Björkman E., Lilliestråle M. and Hedin N. 2013. Activated carbons prepared from hydrothermally carbonized waste biomass used as adsorbents for CO2, Appl. Energy, 112, 526–532.

22. Xu J., Shi J., Cui H., Yan N. and Liu Y. 2018. Preparation of nitrogen doped carbon from tree leaves as efficient CO2 adsorbent, Chem. Phys. Lett., 711, 107–112.

23. Serafin J., Narkiewicz U., Morawski A. W., Wróbel R. J., and Michalkiewicz B. 2017. Highly microporous activated carbons from biomass for CO2 capture and effective micropores at different conditions, J. CO2 Util., 18, 73–79.

24. Guo L., Yang J., Hu G., Hu X., Wang L., Dong Y., DaCosta H., Fan M. 2016. Role of hydrogen peroxide preoxidizing on CO2 adsorption of nitrogen-doped carbons produced from coconut shell, ACS Sustain. Chem. Eng., 4(5), 2806–2813.

25. Chen J., Yang J., Hu G., Hu X., Li Z., Shen S., Radosz M., Fan M. 2016. Enhanced CO2 capture capacity of nitrogen-doped biomass-derived porous carbons, ACS Sustain. Chem. Eng., 4(3), 1439–1445.

26. Yue L., Xia Q., Wang L., Wang L., DaCosta H., Yang J., Hu X. 2018. CO2 adsorption at nitrogen-doped carbons prepared by K2CO3 activation of urea-modified coconut shell, J. Colloid Interface Sci., 511, 259–267.

27. Parshetti G. K., Chowdhury S. and Balasubramanian R. 2015. Biomass derived low-cost microporous adsorbents for efficient CO2 capture, Fuel, 148, 246–254.

28. Han J., Zhang L., Zhao B., Qin L., Wang Y. and Xing F. 2019. The N-doped activated carbon derived from sugarcane bagasse for CO2 adsorption, Ind. Crops Prod., 128, 290–297.

29. Huang G., Liu Y., Wu X. and Cai J.2019. Activated carbons prepared by the KOH activation of a hydrochar from garlic peel and their CO2 adsorption performance, New Carbon Mater., 34(3), 247–257.

30. Pang R., Lu T., Shao J., Wang L., Wu X., Qian X., Hu X. 2020. Highly efficient nitrogen-doped porous carbonaceous CO2 adsorbents derived from biomass, Energy & Fuels, 35(2), 1620–1628.

31. Coromina H. M., Walsh D. A. and Mokaya R. 2016. Biomass-derived activated carbon with simultaneously enhanced CO2 uptake for both pre and post combustion capture applications, J. Mater. Chem. A, 4(1), 280–289.

32. González B. and Manyà J. J. 2020. Activated olive mill waste-based hydrors as selective adsorbents for CO2 capture under postcombustion conditions, Chem. Eng. Process. Intensif., 149, 107830.

33. Li K., Tian S., Jiang J., Wang J., Chen X. and Yan F. 2016. "Pine cone shell-based activated carbon used for CO 2 adsorption," J. Mater. Chem. A, 4(14), 5223–5234.

34. Deng S., Wei H., Chen T., Wang B., Huang J. and Yu G. 2014. Superior CO2 adsorption on pine nut shell-derived activated carbons and the effective micropores at different temperatures, Chem. Eng. J., 253, 46–54.

35. Li D., Ma T., Zhang R., Tian Y., and Qiao Y. 2015. Preparation of porous carbons with high low-pressure CO2 uptake by KOH activation of rice husk char, Fuel, 139, 68–70.

36. Ding S. and Liu Y. 2020. Adsorption of CO2 from flue gas by novel seaweed-based KOH-activated porous biochar, Fuel, 260, 116382.

37. Zhao Z., Ma C., Chen F., Xu G., Pang R., Qian X., Shao J., Hu X. 2021. Water caltrop shell-derived nitrogen-doped porous carbons with high CO2 adsorption capacity, Biomass and Bioenergy, 145, 105969. doi: https://doi.org/10.1016/j.biombioe.2021.105969

38. Li Q., Liu S., Peng W., Zhu W., Wang L., Chen F., Shao J., Hu X. 2020.Preparation of biomass-derived porous carbons by a facile method and application to CO2 adsorption, J. Taiwan Inst. Chem. Eng., 116, 128–136. doi: https://doi.org/10.1016/j.jtice.2020.11.001

39. Deana Q., Nor Mohd R. N., Azil B. A., Hamasa K. and Nurul S. A. A. 2023. Adsorption of hydrogen sulphide (H2S) using xerogel synthesized from palm kernel shell biochar, Mater. Res. Proc., 29, 109–116. doi: https://doi.org/10.21741/9781644902516-14

40. Imoisili P. E., Ukoba K. O. and Jen T.-C. 2020. Green technology extraction and characterisation

of silica nanoparticles from palm kernel shell ash via sol–gel, J. Mater. Res. Technol., 9(1), 307–313.

41. Lopes J. M., Mustapa A. N., Pantić M., Bermejo M. D., Martín Á., Novak Z., Knez Ž., Cocero M. J. 2017. Preparation of cellulose aerogels from ionic liquid solutions for supercritical impregnation of phytol, J. Supercrit. Fluids, 130, 17–22. doi: https://doi.org/10.1016/j.supflu.2017.07.018

42. Noraini N. M. R., Alias A. B., Qarizada D., Azman F. A. M., Rashid Z. A., and Hasan M. R. C. 2022. Synthesis and Characterization of Xerogel from Palm Kernel Shell Biochar, J. Mech. Eng., 11(1), 211–226. doi: https://doi.org/10.24191/jmeche.v11i1.23599

43. Quan C., Zhou Y., Wu C., Xu G., Feng D., Zhang Y., Gao N. 2023. Valorization of solid digestate into activated carbon and its potential for CO2 capture, J. Anal. Appl. Pyrolysis, 169, 105874. doi: https://doi.org/10.1016/j.jaap.2023.105874

44. Of O. 2017. Characterization of activated carbon using chemical activation via microwave ultrasonic system (Pencirian Karbon Teraktif Menggunakan Sistem Pengaktifan Kimia Melalui Ketuhar, 21(1), 159–165.

45. Al Malki M., Yaser A. Z., Hamzah M. A. A. M., Zaini M. A. A., Latif N.A., Hasmoni S.H., Zakaria Z.A. 2023. Date Palm Biochar and Date Palm Activated Carbon as Green Adsorbent—Synthesis and Application, Curr. Pollut. Reports, 9(3), 374–390, doi: https://doi.org/10.1007/s40726-023-00275-6

46. Yasin N. M. F. M., Meri N. H., Talib N., Ghani W. A. W. A. K., Rashid Z. A. and Alias A. B. 2021. Breakthrough Analysis of Empty Fruit Bunch-Based Hydrogel Biochar Composite (EFB-HBC) for Hydrogen Sulphide (H 2 S) Adsorption Study Removal, 200, ICoST, 216–225, doi: https://doi.org/10.2991/aer.k.201229.030

47. Kumar A. and Jena H. M. 2016. Preparation and characterization of high surface area activated carbon from Fox nut (Euryale ferox) shell by chemical activation with H3PO4, Results Phys., 6, 651–658, doi: https://doi.org/10.1016/j.rinp.2016.09.012

48. Supian M. A. F., Amin K. N. M., Jamari S. S. and Mohamad S. 2020. Production of cellulose nanofiber (CNF) from empty fruit bunch (EFB) via mechanical method, J. Environ. Chem. Eng., 8(1), 103024, doi: https://doi.org/10.1016/j.jece.2019.103024

49. Kunusa W. R., Iyabu H. and Abdullah R. 2021. FTIR, SEM and XRD analysis of activated carbon from sago wastes using acid modification, J. Phys. Conf. Ser., 1968(1). doi: https://doi.org/10.1088/1742-6596/1968/1/012014

50. Alias A. B. and Qarizada D. 2022. Comparison of hydrogel- and xerogel- based sorbent from Empty Fruit Bunch, 118(2), 49–60. doi: https://doi.org/10.5604/01.3001.0016.2579

51. Maulina S. and Mentari V. A. 2019. Comparison of Functional Group and Morphological Surface of Activated Carbon from Oil Palm Fronds Using Phosphoric Acid (H3PO4) and Nitric Acid (HNO3) as an Activator, IOP Conf. Ser. Mater. Sci. Eng., 505(1), doi: https://doi.org/10.1088/1757-899X/505/1/012023

52. Amosa M. K. 2015. Environmental Nanotechnology, Monitoring & Management Process optimization of Mn and H 2 S removals from POME using an enhanced empty fruit bunch (EFB) -based adsorbent produced by pyrolysis, Environ. Nanotechnology, Monit. & Manag., 493–105. doi: https://doi.org/10.1016/j.enmm.2015.09.002

53. Glaser R., Iyabu H., Abdullah R. 2021. FTIR, SEM and XRD analysis of activated carbon from sago wastes using acid modification FTIR, SEM and XRD analysis of activated carbon from sago wastes using acid modification, doi: https://doi.org/10.1088/1742-6596/1968/1/012014

54. Research article production and characterization of activated carbon from. 2018. 5(1–8).

55. Wang X., Zhang Y., Jiang H., Song Y., Zhou Z. and Zhao H. 2016. Author 's Accepted Manuscript, Mater. Lett., doi: https://doi.org/10.1016/j.matlet.2016.07.081

56. Segovia-sandoval S. J., Pastrana-martínez L. M., Ocampo- R., Morales-Torres S. and Berber-Mendoza M. S. 2019. Synthesis and characterization of carbon xerogel/graphene hybrids as adsorbents for metronidazole pharmaceutical removal: effect of operating parameters, Sep. Purif. Technol., 116341. doi: https://doi.org/10.1016/j.seppur.2019.116341

57. Lee S., Lee S. and Roh J. 2021. Analysis of Activation Process of Carbon Black Based on Structural Parameters Obtained by XRD Analysis, 1–11.

58. Shah M. S., Tsapatsis M., and Siepmann J. I. 2017. Hydrogen Sul fi de Capture : From Absorption in Polar Liquids to Oxide, Zeolite, and Metal − Organic Framework Adsorbents and Membranes, doi: https://doi.org/10.1021/acs.chemrev.7b00095

59. Guzel G. and Deveci H. 2020. Effect of Aging Solvents on Physicochemical and Thermal Properties of Silica Xerogels Derived from Steel Slag, 1586–1591. doi: https://doi.org/10.1002/slct.201903345

60. Meri N. H., Alias A. B., Rashid Z. A. and Wan W. A. Karim Ghani A.B. 2018. Effect of Chemical Washing Pre-treatment of Empty Fruit Bunch (EFB) biochar on Characterization of Hydrogel Biochar composite as Bioadsorbent, IOP Conf. Ser. Mater. Sci. Eng., 358, 1–7. doi: https://doi.org/10.1088/1757-899X/358/1/012018